Chemical Science

Accepted Manuscript

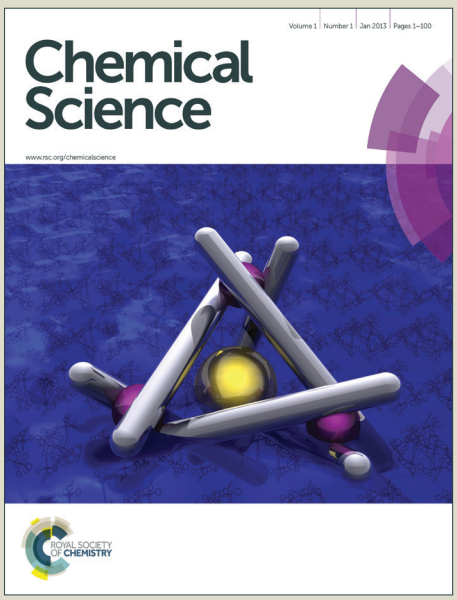

ROYAL SOCIETY OF CHEMISTRY

www.rsc.org/chemicalscience

Journal Name

RSCPublishing

EDGE ARTICLE

Shape and Composition Control of $Bi_{19}S_{27}(Br_{3-x}I_x)$ Alloyed Nanowires: The Role of Metal Ions†

Cite this: DOI: 10.1039/x0xx00000x

Yihui Wu,[a] Huanhuan Pan,[b] Xin Zhou,[a] Mingrun Li,[a] Bin Zhou,[a] Chi Yang,[a,c] Wen-Hua Zhang,*[a] Jiansheng Jie*[b] and Can Li*[a]

Received ooth January 2015,
Accepted ooth January 2015

DOI: 10.1039/x0xx00000x

www.rsc.org/

We present the first colloidal synthesis of highly uniform single-crystalline $Bi_{19}S_{27}Br_3$ nanowires (NWs) with the mean diameters of ~9 nm and tunable length in the range of 0.15–2 μm in the presence of foreign metal ions (Al^{3+}). The Al^{3+} ions not only control the growth of NWs, but also achieve species transformation, *i.e.*, from Bi_2S_3 to $Bi_{19}S_{27}Br_3$, while they are not presented in the resulting NWs. This colloidal chemistry approach can be expanded to prepare a family of single-crystalline $Bi_{19}S_{27}(Br_{3-x,}I_x)$ alloyed NWs with controlled compositions ($0 \leq x \leq 3$). Interestingly, these alloyed NWs show an unusual composition-independent band gap of ~0.82 eV, and the theoretical calculation indicates that this phenomenon comes from the very minor contributions of halogen to the valence band maximum and conduction band minimum. The photodetectors made of the $Bi_{19}S_{27}(Br_{3-x,}I_x)$ alloyed NWs show a pronounced photoresponse with high stability and reproducibility, which makes the NWs potentially useful candidates in optoelectronic devices.

Introduction

Semiconductor nanowires (NWs),[1] which are key building blocks for the next generation of optoelectronic devices, such as light-emitting diodes (LEDs),[2] solar cells,[3] photodetectors,[4] field-effect transistors (FETs),[5] thermoelectrics,[6] and so on, have been extensively studied due to their anisotropic geometry, large surface-to-volume ratio, the decoupling of light absorption and minority carrier diffusion directions for efficient charge collection and separation, and the exciton confinement in two dimensions that are superior to their bulk counterparts. Moreover, semiconductor NWs have various mechanical properties and reactivity which depend on the crystallographic orientation.[7] Considerable efforts have been made to exploit their useful properties, and widen their applications, especially to improve their synthesis,[1a,8] such as metal-nanoparticle-mediated methods,[9] direct deposition methods,[10] template-directed methods,[11] and oriented-attachment methods in colloidal chemistry.[12] Colloidal synthesis, which takes advantages of the versatility of the precursors, ligand affinity, solvent polarity, and reactions parameters, has been demonstrated to be a powerful strategy to exploit colloidal nanocrystals (NCs) with controlled phases,[13] morphology[14] and composition[15] for binary and ternary systems, and even . Superiority of colloidal chemistry has also been demonstrated in synthesis of very interesting semiconductoring heterostructured NCs.[16] In contrast, the controllable synthesis of quaternary and quinary alloyed NCs is much more difficult, and the synthesis of multi-component NWs meets even bigger challenge than nanoparticles. Generally, long carbon chain organic molecules that selectively bind to different NC facets are used to control the morphology of the resulting NCs.[17] Most recently, inorganic foreign metal ions have been employed to influence the morphology of semiconductor NCs (Cu_xSe and CuTe NCs),[18] which may provide a new way to achieve the shape control of NCs. However, no success has been reported on the formation of one-dimensional nanomaterials mediated by foreign metal ions up to data, let alone multi-component NWs. This inspires us to employ this strategy to exploit new type of multi-component semiconductor NWs, which may greatly expand the research platform in this field.

A group of $Bi^{III}VI^{A}VII^{A}$ compounds, BiOCl, BiSCl, $Bi_{19}S_{27}Br_3$, and BiSI, had evoked great research interest varying from catalysis to electronics due to their promising properties, such as optoelectrical effect, photoconductivity, ferroelectricity, piezoelectricity, electromechanical effect, and a large temperature dependence of the band gap.[19] Traditionally, these semiconductors with poor-defined morphology were synthesized via vapor-phase growth at high temperature (> 600 °C), which usually required special and complicated facility and

[a]*State Key Laboratory of Catalysis, Dalian Institute of Chemical Physics, Chinese Academy of Sciences; Dalian National Laboratory for Clean Energy, Dalian 116023, China E-mail: whzhang@dicp.ac.cn; canli@dicp.ac.cn*
[b]*Institute of Functional Nano & Soft Materials (FUNSOM), Collaborative Innovation Center of Suzhou Nano Science and Technology, Soochow University, Suzhou Jiangsu 215123, China E-mail: jsjie@suda.edu.cn*
[c]*Department of Materials Science and Engineering, University of Science and Technology of China, Hefei 230026,China*
†*Electronic Supplementary Information (ESI) available: experimental details, XRD patterns, TEM and HRTEM images, energy-dispersive X-ray spectra, UV–vis spectra, and Tauc plots. See DOI: 10.1039/c000000x/*

even toxic H_2S and HBr.[20] Solvothermal method has been exploited to prepare bundle-rodlike $Bi_{19}S_{27}Br_3$.[19c] A microwave-assistant aqueous synthesis has recently been developed to prepare fabric-like $Bi_{19}S_{27}Br_3$ superstructures with large diameters (~80nm) and their photocatalytic performance has also been investigated.[19d] However, to the best of our knowledge, controllable synthesis of single-crystalline $Bi_{19}S_{27}Br_3$ colloidal NWs with uniform morphology remains undeveloped, hindering understanding of their fundamental properties and exploiting their potential applications. Herein we present a facile, colloidal approach to well-defined $Bi_{19}S_{27}Br_3$ NWs by using Al^{3+} ions to mediate the oriented growth of $Bi_{19}S_{27}Br_3$. We have demonstrated that aluminum(III) acetylacetonate [$Al(acac)_3$] not only control the growth of NWs, but also achieve species transformation, *i.e.*, from Bi_2S_3 to $Bi_{19}S_{27}Br_3$. We have further expanded this foreign metal ions mediated approach to realize the synthesis of uniform quaternary $Bi_{19}S_{27}(Br_{3-x},I_x)$ NWs with compositions varied across the entire ranges ($0 \le x \le 3$). Full experimental details can be found in the Electronic Supplementary Information (ESI†). Their microstructures and properties were thoroughly characterized by a variety of spectroscopy, such as X-ray diffraction (XRD), X-ray photoelectron spectroscopy (XPS), Raman spectra, scanning electron microscopy (SEM), transmission electron microscopy (TEM), high-resolution transmission electron microscopy (HRTEM), and UV-visible-near-infrared (UV-vis-NIR) absorption spectroscopy. It is very interesting to find that these alloyed NWs show an unusual composition-independent band gap, which differs from the widely accepted Vegard's Law for multi-component alloyed semiconductors.[21] The application potential of $Bi_{19}S_{27}(Br_{3-x},I_x)$ NWs in photoelectronics was finally assessed by fabricating photodetectors (PDs), showing a pronounced photoresponse with high stability.

Results and discussion

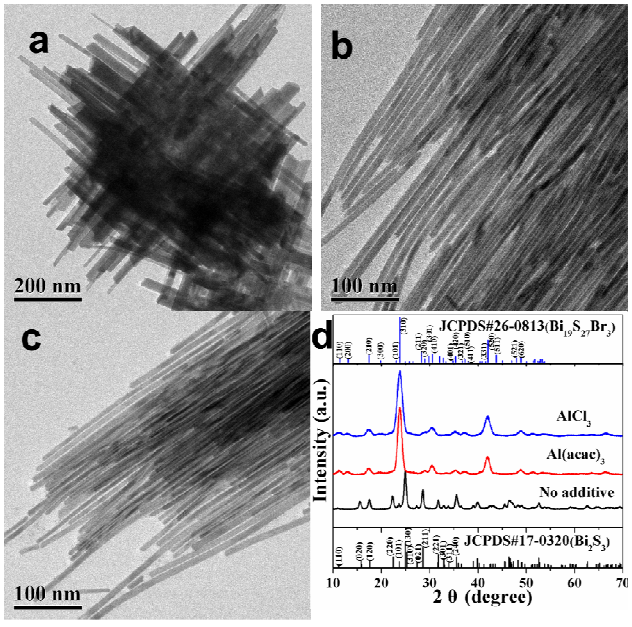

Fig. 1 TEM images of the as-synthesized NWs obtained by adding different salts into the reaction mixtures: a) no additive, b) $Al(acac)_3$, c) $AlCl_3$, and d) the corresponding XRD patterns of the three materials.

Fig. 1a shows the TEM image of the sample prepared in the absence of Al^{3+}. The product was assemble of fabric-like NWs with diameters varying in a wide range, which was revealed to be orthorhombic Bi_2S_3 (JCPDS No. 17-0320) by XRD (Fig. 1d). The high-angle annular dark-field-scanning transmission microscopy (HAADF-STEM) and TEM image reveals the fabric-like morphology of Bi_2S_3 should be formed via physical crossover of nonuniform NWs (Fig. S1, ESI†). High resolution TEM (HRTEM) images along with the corresponding fast Fourier transform (FFT) pattern confirm the single crystalline nature of the product (Fig. S1, ESI†). Very interestingly, the presence of $Al(acac)_3$ in the synthesis medium resulted in hexagonal-structured $Bi_{19}S_{27}Br_3$ NWs (JCPDS No. 26-0813) with mean diameters of ~9.0 nm, as shown in Fig. 1b

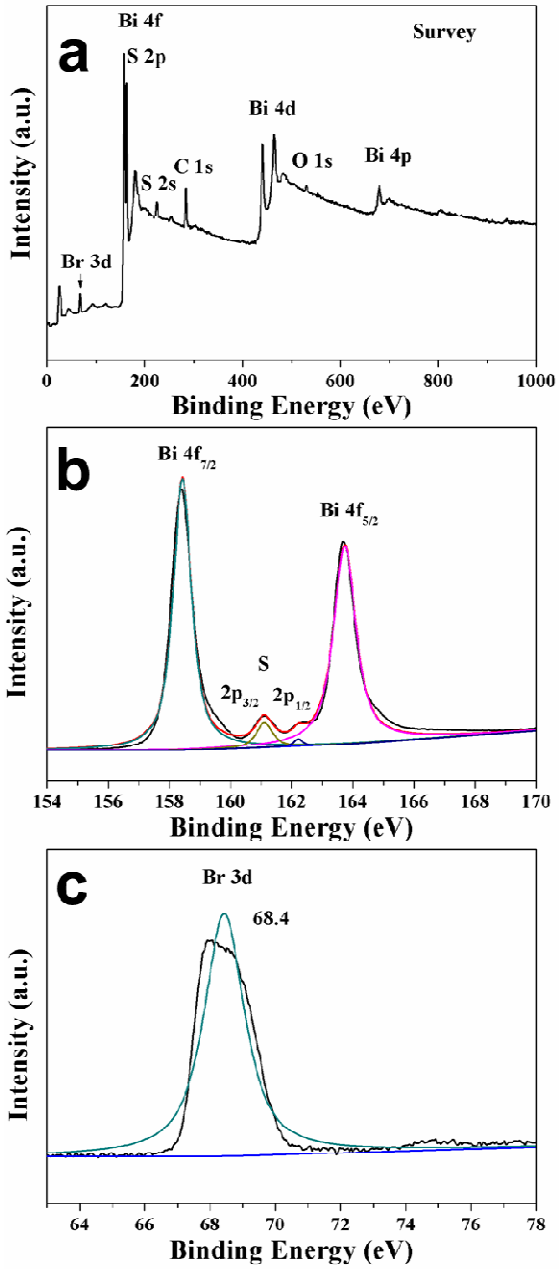

Fig. 2 XPS spectra of $Bi_{19}S_{27}Br_3$ NWs: a) survey XPS spectrum, b) high-resolution spectra of Bi 4f and S 2p, and c) high-resolution spectrum of Br 3d.

(TEM) and 1d (XRD). It is noteworthy that the length of the as-synthesized $Bi_{19}S_{27}Br_3$ NWs can be tuned in the range of 0.15–2 μm by varying the reaction duration while the mean diameters do not change apparently (Fig. S2, ESI†, the reaction temperature was kept at 180 °C). Moreover, the mean diameters can be tuned from ~6.9 nm to ~12 nm by varying the reaction temperatures while the length of the NWs remain basically unchanged (Fig. S3, ESI†, the reaction time was kept at 30 min). Therefore, the presence of $Al(acac)_3$ was critical to the formation of $Bi_{19}S_{27}Br_3$ NWs and the reaction conditions were important to produce the NWs with narrow size distributions. To ascertain whether it is the Al^{3+} that plays the key role in formation of well-defined $Bi_{19}S_{27}Br_3$ NWs, $AlCl_3$ was used as additive to replace $Al(acac)_3$ in the synthesis process, hexagonal $Bi_{19}S_{27}Br_3$ NWs with very similar morphology were again obtained (Fig. 1c and 1d), as the case in the presence of $Al(acac)_3$. Therefore, Al^{3+} ions can achieve not only the morphology control, but also the species transformation, *i.e.* , from Bi_2S_3 to $Bi_{19}S_{27}Br_3$ in this case. To investigate the NWs composition, energy dispersive X-ray spectroscopy (EDS) was performed (Table S1, ESI†), showing the ratio of Bi:S:Br was approximately 19:26:5. Thus the as-synthesized NWs are slightly sulfur poor and bromine rich. However, EDS can not detect the presence of Al element in the NWs. X-ray photoelectron spectroscopy (XPS) was further employed to characterize the $Bi_{19}S_{27}Br_3$ NWs (Fig. 2), displaying peaks centred at 158.4 eV and 163.7 eV, which corresponded to the Bi $4f_{7/2}$ and Bi $4f_{5/2}$ of Bi^{3+} ions,[22] respectively. The peaks centred at 161.1 eV and 162.2 eV overlapped with Bi 4f were assigned to S $2p_{3/2}$ and S $2p_{1/2}$ of S^{2-} ions,[22b,23] respectively. The signal with binding energy of 68.4 eV is characteristic of Br^- ions (Br 3d). Altogether, the above data confirm that the $Bi_{19}S_{27}Br_3$ NWs obtained through our colloidal approach is phase pure.

The influence of the concentration of Al^{3+} ions on the dimension of the resulting $Bi_{19}S_{27}Br_3$ NWs was further studied by adding different amounts of Al^{3+} ions in the synthesis. It was found that the length of the $Bi_{19}S_{27}Br_3$ NWs was gradually decreased to a certain degree upon increasing the dosages of Al^{3+} ions, while the mean diameters of the $Bi_{19}S_{27}Br_3$ NWs remain constant (Fig. S4, ESI†). The role of Al^{3+} ions in shape control over the $Bi_{19}S_{27}Br_3$ NWs is probably proceeded by promoting the crystal growth in a specific direction,[18b] the corresponding growth mechanisms of the NWs were shown in Scheme 1. If more Al^{3+} ions present in the reaction mixture, the Bi precursors will be divided into more regions, and more nucleation sites will be generated, resulting in the formation of shorter NWs. However, the transformation mechanism from Bi_2S_3 to $Bi_{19}S_{27}Br_3$ is needed to be elucidated in this study. It is proposed that Al^{3+} would compete with Bi^{3+} in adsorbing S^{2-} in reaction system, which may reduce the reaction probability between Bi^{3+} and S^{2-}, leading to an incomplete replacement of Br^- by S^{2-}, thus forming the hexagonal structured $Bi_{19}S_{27}Br_3$. Another possible explanation is that, during the NW synthesis, $BiBr_3$ and $Al(acac)_3$ were simultaneously dissolved in ODE solution, and they should exist in molecular form. $BiBr_3$ molecules may be surrounded by some Al^{3+} via the electrostatic force between Br^- and Al^{3+}. In such case, Al^{3+} can form a screen to suppress, to a certain degree, the attack of S^{2-} to $BiBr_3$, thus a portion of Br^- was retained in reaction intermediate, leading to the formation of a new species $Bi_{19}S_{27}Br_3$. Deep understanding of the growth process is very complicated, further study should be performed with aid of theoretical calculation. If any of the above explanations is true, it could be expected that other cations should also exert similar influence on the reaction of nanowire growth in this study. We have hence chosen Fe^{3+}, Fe^{2+}, Co^{3+}, Co^{2+}, and Ni^{2+} ions to investigate the influence of foreign metal ions on this reaction. Indeed, these cations function almost the same as Al^{3+} ions in the formation of $Bi_{19}S_{27}Br_3$. The corresponding TEM images and XRD patterns for these nanowires are shown in Fig. S5 and Fig. S6, ESI†, respectively.

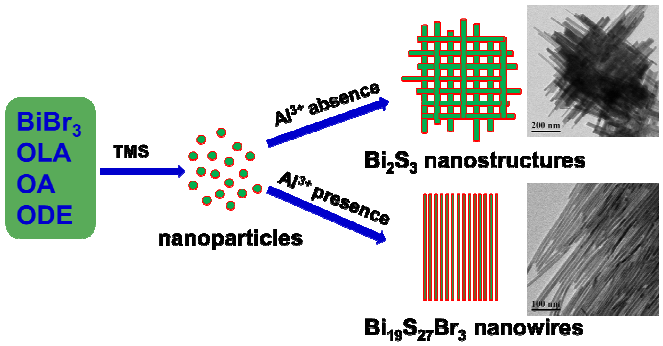

Scheme 1 Schematic illustration for the proposed formation process of $Bi_{19}S_{27}Br_3$ nanowires. (OLA: oleylamine, OA: oleic acid, ODE: 1-Octadecene)

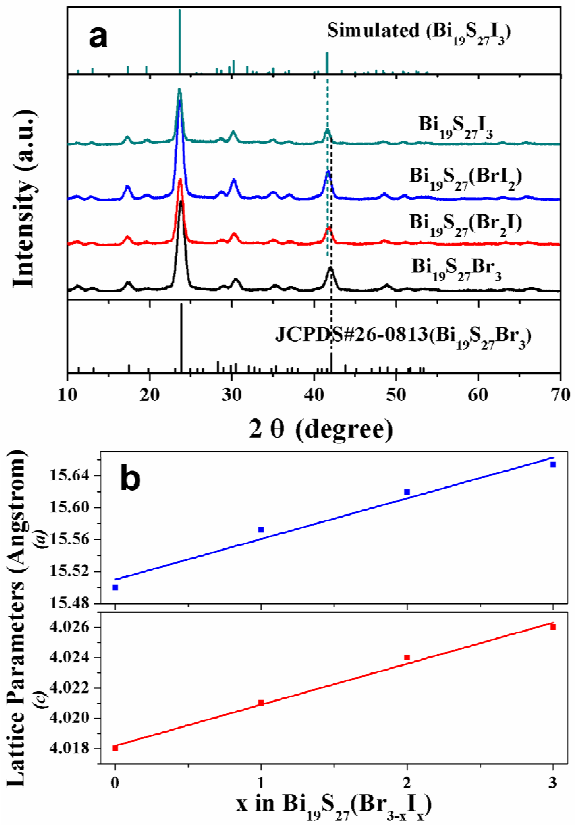

Fig. 3 XRD patterns (a) and Vegard's plot (b) of $Bi_{19}S_{27}(Br_{3-x},I_x)$ with various I/(Br+I) ratios ($0 \le x \le 3$).

To expand the present synthesis of $Bi_{19}S_{27}Br_3$ NWs to other $Bi^{III}VI^{A}VII^{A}$ materials, we have further prepared $Bi_{19}S_{27}(Br_{3-x},I_x)$ ($0 \le x \le 3$) alloyed NWs. Fig. 3a presents XRD patterns of the as-

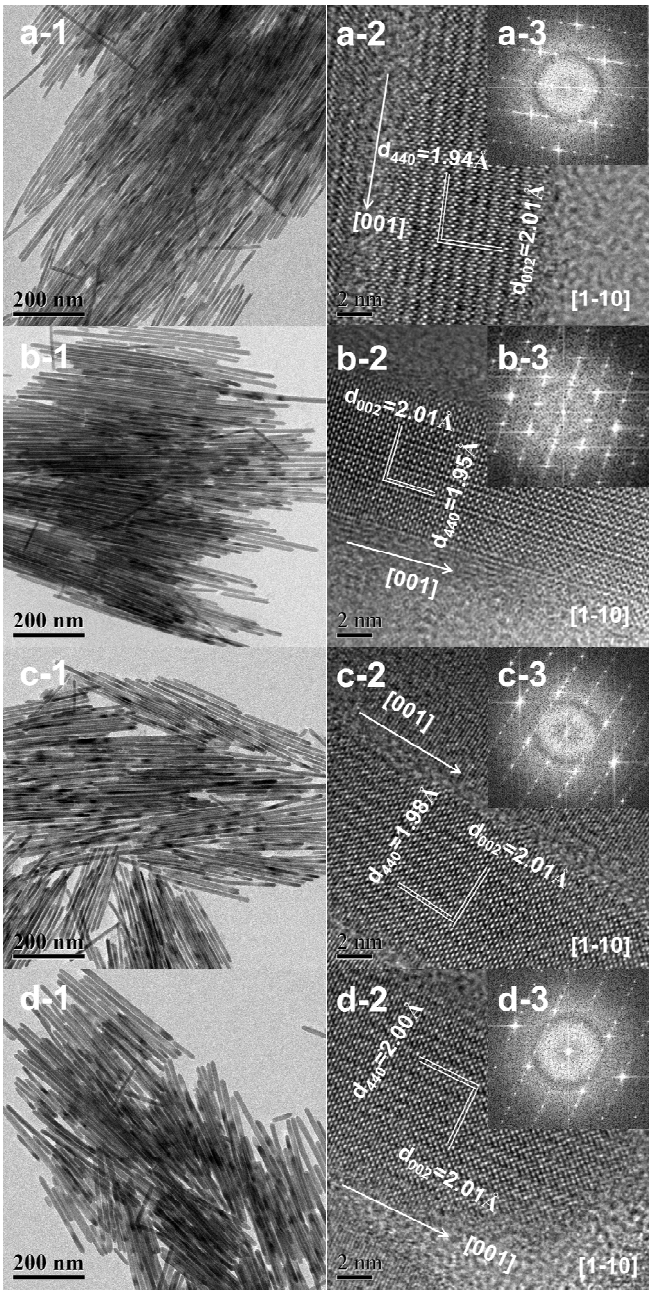

Fig. 4 TEM analysis of the $Bi_{19}S_{27}(Br_{3-x},I_x)$ (0≤ x ≤3) NWs. a), b), c), and d) denote respectively the samples $Bi_{19}S_{27}Br_3$, $Bi_{19}S_{27}(Br_2I)$, $Bi_{19}S_{27}(BrI_2)$, and $Bi_{19}S_{27}I_3$ NWs. 1, 2, and 3 represent the corresponding low magnification TEM images, HRTEM images and corresponding FFT patterns for these samples.

synthesized $Bi_{19}S_{27}(Br_{3-x},I_x)$ NWs ($0 \le x \le 3$). For $Bi_{19}S_{27}I_3$, the XRD pattern does not match any existing patterns in the standard JCPDS database, thus a diffraction pattern for hexagonal $Bi_{19}S_{27}I_3$ was simulated on the basis of $Bi_{19}S_{27}Br_3$ crystal structure by substituting the Br^- lattices position with I^- (Table S2, ESI†). The lattice constants calculated from the experimental diffraction pattern (a = 15.65 Å and c = 4.026 Å) were used in this simulation. The d-spacings of the experimental reflections matches well with the simulated ones, indicating that the $Bi_{19}S_{27}I_3$ NWs should exhibit the same hexagonal structure as $Bi_{19}S_{27}Br_3$ NWs. Additionally, the major diffraction peaks shift systematically toward lower angles with increasing the contents of I, meaning that the larger I atoms have gradually replaced the smaller Br atoms in the lattices of the resulting NWs. More importantly, no additional peak or peak splitting can be detected by XRD, ruling out the possibility of phase separation or separation nucleation that often occurs in preparation of alloyed nanocrystals.[21b] Vegard's graph (Fig. 3b) obtained by plotting the lattice parameter values (a and c) versus compositions show close to linear trend with increasing iodine content, confirming the formation of a solid solution. Raman spectroscopy is a sensitive tool to reflect phase purity of a material. The Raman spectra of the as-prepared NWs in Fig. S7, ESI† show five peaks, located at 127, 145, 192, 217 and 270 cm^{-1}, respectively. The strongest Raman peak at ~270 cm^{-1} can be assigned the motion between the Bi and S atoms as well as the Br atom at rest for that $Bi_{19}S_{27}Br_3$ NW. The absence of the Bi_2S_3 signals[24] around 185, 236 and 260 cm^{-1}, and the $BiBr_3$ peaks,[25] around 143, 156 and 173 cm^{-1} confirmed the high purity of the $Bi_{19}S_{27}Br_3$ NWs obtained in this study. Similar scenarios occurred for other three samples with varied I/Br ratios. Therefore, we have successfully synthesized pure phase $Bi_{19}S_{27}(Br_{3-x},I_x)$ NWs with characteristics that the chemical compositions can be consecutively tailored across the entire compositional range ($0 \le x \le 3$).

TEM and SEM were then performed to reveal the morphology and microstructures of the $Bi_{19}S_{27}(Br_{3-x},I_x)$ alloyed NWs, as shown in Fig. 4 and Fig. S8, ESI†, respectively. The low-magnification TEM and SEM images display a uniform diameter distributions of the $Bi_{19}S_{27}(Br_{3-x},I_x)$ NWs, and the diameters increase gradually from ~9.0 to ~13.9 nm with increasing I contents (Fig. S9, ESI†). It is well-known that, to decrease system energy, the facets with lower energy would gradually grow larger, while the facets with higher energy gradually get smaller, and even disappear during crystal growth. To gain insight into the variations in the diameters of the $Bi_{19}S_{27}(Br_{3-x},I_x)$ NWs in this study, theoretical evaluation of surface energy of NW facets was carried out. The diameters of the hexagonal $Bi_{19}S_{27}(Br_{3-x},I_x)$ NWs should be influenced significantly by the relative surface energies of (110) facet/(001) facet. This data is estimated to be 2.34 for the $Bi_{19}S_{27}I_3$ NWs, which is significantly higher than the 0.71 for the $Bi_{19}S_{27}Br_3$ NWs. This means that, in comparison with the $Bi_{19}S_{27}Br_3$ NWs, the $Bi_{19}S_{27}I_3$ NWs with larger (001) facets exhibit lower system energy. The (001) facet of the $Bi_{19}S_{27}I_3$ would grow larger while (110) facet become smaller. Therefore, the diameters of $Bi_{19}S_{27}(Br_{3-x},I_x)$ NWs increase gradually when the I contents were increased. High-resolution TEM (HRTEM) images show that all $Bi_{19}S_{27}(Br_{3-x},I_x)$ NWs are highly crystalline with continuous lattice fringes and the corresponding fast Fourier transform (FFT) pattern on a single NW confirm the single crystalline nature. The lattice distance of 0.201 nm matches well with the (002) plane of the hexagonal $Bi_{19}S_{27}Br_3$, indicating that the growth of NWs is oriented along the [001] direction. Moreover, the interplanar crystal spacing of d_{440} increase from 0.194 nm to 0.200 nm with increasing the I contents, meaning again that the larger I atoms have successfully replaced the smaller Br atoms in the lattices of the resulting NWs, which is in good agreement with the XRD results. Elemental analysis by EDS (Table S1 and Fig. S10, ESI†) shows that increasing of the I contents was accompanied by decreasing the Br contents in the ranges of $0 \le x \le 3$ for the as-prepared $Bi_{19}S_{27}(Br_{3-x},I_x)$ NWs. Moreover, the elemental mapping and line scan (Fig. 5) of $Bi_{19}S_{27}(BrI_2)$ NWs confirm the homogeneous distribution of the four elements contained. These

results demonstrate the formation of alloyed NWs with homogeneous distribution of Br and I in the $Bi_{19}S_{27}(Br_{3-x},I_x)$ matrix.

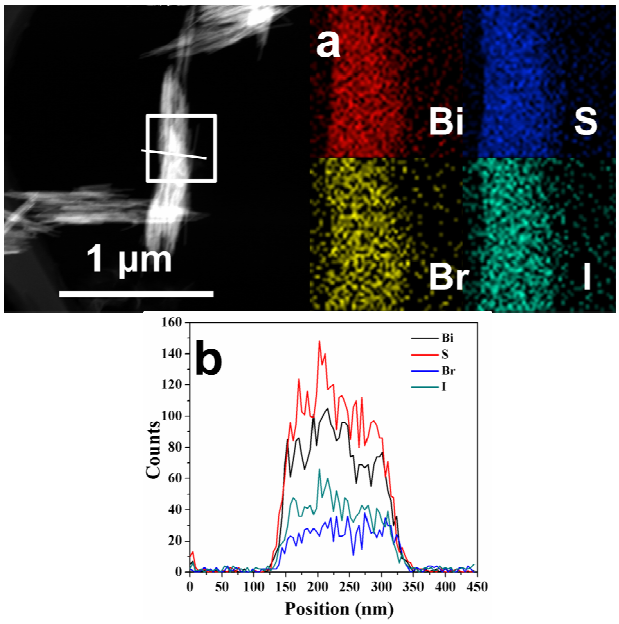

Fig. 5 HAADF-STEM image and corresponding EDS elemental mapping (a) and STEM-EDS line scan (b) of $Bi_{19}S_{27}(BrI_2)$ NWs.

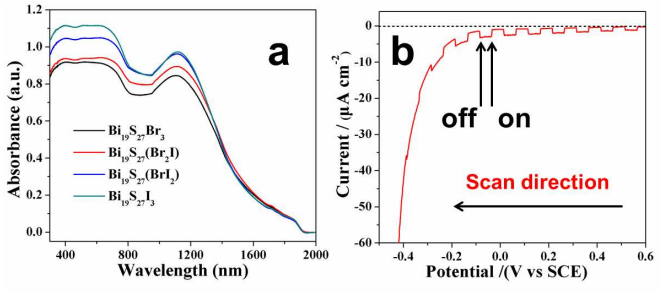

Fig. 6 (a) UV-vis-NIR diffuse-reflectance spectra (DRS) of $Bi_{19}S_{27}(Br_{3-x},I_x)$ ($0 \le x \le 3$) NWs, (b) Transient photocurrent response of the $Bi_{19}S_{27}(Br_2I)$ NWs.

The UV-vis-NIR diffuse-reflectance spectroscopy (DRS) spectra of the $Bi_{19}S_{27}(Br_{3-x},I_x)$ NWs ($0 \le x \le 3$) were measured to study their optical properties (Fig. 6a). A continuous strong absorption spanning the whole visible to near IR spectrum is found. It is noteworthy that the absorption intensity increases gradually along with increasing I contents. Tauc plots (Fig. S11, ESI†) were performed to determine the optical band gaps with a relationship of the α^2 versus the energy, revealing that $Bi_{19}S_{27}Br_3$ NWs exhibits a direct band gap of 0.815 eV. Interestingly, the band gap energies were keep basically unchanged upon varying the ratio of I/Br for the $Bi_{19}S_{27}(Br_{3-x},I_x)$ NWs ($0 \le x \le 3$), meaning that the synthesized NWs exhibit band gap independent of the composition, which is so different from the widely accepted Vegard's Law for multi-component alloyed semiconductors.[21] In order to deeply understand the electronic structure of $Bi_{19}S_{27}Br_3$,

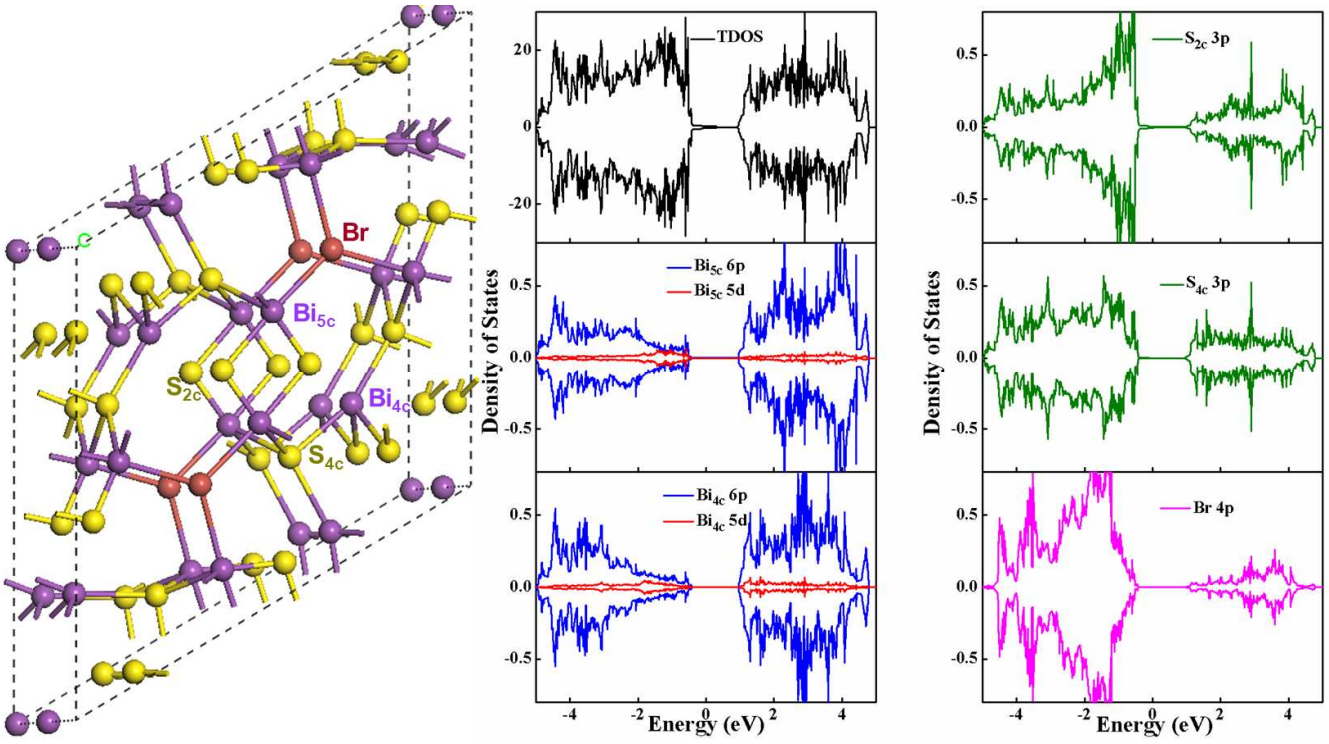

Fig. 7 The structural model and DOS for $Bi_{19}S_{27}Br_3$.

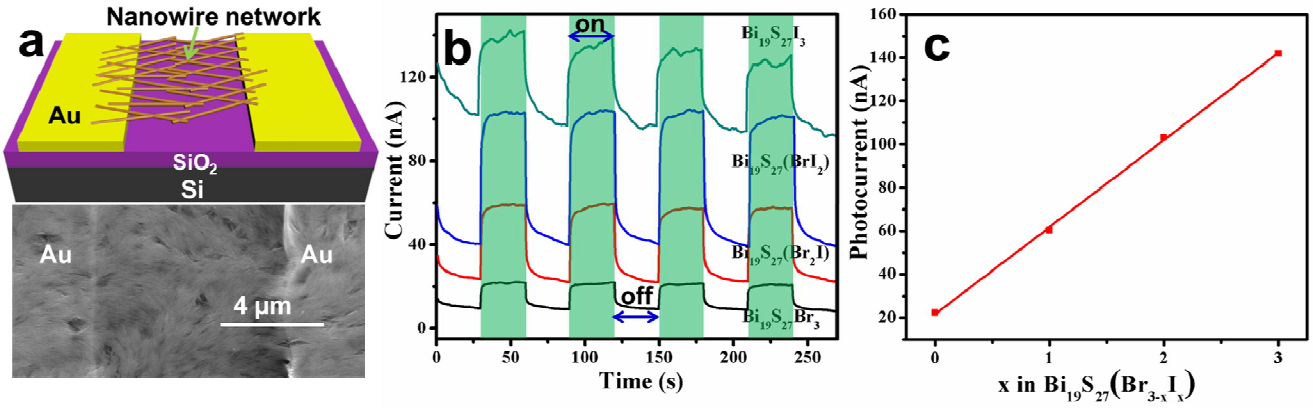

Fig. 8 (a) Schematic illustration of the PD based on the $Bi_{19}S_{27}(Br_{3-x}I_x)$ NW networks (x=0, 1, 2, 3). SEM image of a typical device is shown below. (b) Transient photoresponse of the PDs to pulsed incident light at a bias of +5 V. (c) Photocurrent versus iodine content (x) curve.

density functional theory calculations have been performed with Vienna ab initio simulation package[26] and projector augmented wave method.[27] The generalized gradient approximation (GGA) with the spin polarized Perdew-Burke-Ernzerhof (PBE) functional [28] has been used to relax the structure and compute the density of states. The results in Fig. 7 and Fig. S12, ESI†, show that the valence band maximum of $Bi_{19}S_{27}Br_3$ and $Bi_{19}S_{27}I_3$ is mostly composed of S 3p states and the conduction band minimum mainly consists of Bi 6p states, slightly mixed with S 3p orbitals. In contrast, Br 4p or I 5p orbitals make important contributions to the lower region of valence band (lower than −0.4 eV), which is possibly the reason that the replacement of Br with I doesn't change the band gap of the as-synthesized NWs. The calculated band gap (about 0.6 eV) is smaller than our experimental value (around 0.82 eV) which may be due to the shortcoming of GGA method in underestimating the band gap.

We have also investigated the photoelectrochemical (PEC) properties of the $Bi_{19}S_{27}(Br_{3-x},I_x)$ NWs ($0 \le x \le 3$) by measuring the transient photocurrents of the NWs films on fluorine tin oxide (FTO) in a photoelectrochemical cell. Photocurrent obtained from the $Bi_{19}S_{27}(Br_2I)$ NWs electrodes was negative (cathode current) (Fig. 6b), indicating that the as-synthesized NWs exhibit p-type semiconductor behavior.[29] Constant bias experiment enables a more realistic evaluation of the charge transport dynamics for device applications, We hence carried out such measurement, as shown in Fig. S13, ESI†, the photocurrents of the $Bi_{19}S_{27}(Br_{3-x},I_x)$ NWs film increased rapidly upon receiving illumination, and dropped immediately to their pre-illumination values without apparent degradation over many light on/off cycles. It can also be seen that the photocurrents increased gradually with increasing the contents of I, which may come from the enhanced absorption intensities, as shown in Fig 6a. Therefore, the $Bi_{19}S_{27}(Br_{3-x},I_x)$ NWs ($0 \le x \le 3$) are sensitive to light illumination and are stable under experimental conditions, which is vital for device applications.

The combination of the strong absorption ability in the visible to near IR region of the spectrum and the sensitive response to light illumination makes the $Bi_{19}S_{27}(Br_{3-x},I_x)$ NWs ($0 \le x \le 3$) excellent candidates for photodetectors (PDs). The as-synthesized alloyed NWs were directly drop-casted on the pre-prepared Au electrode (50 nm) pairs on SiO_2 (300 nm)/p^+-Si substrate. Fig. 8a shows the schematic illustration and a representative SEM image of the PD based on the NW network. Despite the short length and small diameter of the NWs, the NWs in the network can connect each other and successfully across the electrode pairs. Current *versus* voltage (*I-V*) curves of the four kinds of PDs measured in the dark are plotted in Fig. S14, ESI†. The linear shapes of the curves demonstrate an ohmic contact of the NW networks with the Au electrodes. Significantly, under the white light illumination (60 mW/cm^2), all the devices show pronounced photoresponses (Fig. 8b), and the devices can be reversibly switched between low- and high-conduction states when the light is switched off and on repeatedly, revealing the high stability and reproducibility of the PDs. Close investigation of the on/off curves reveals that (Fig. 8c), the highest photocurrents for the PDs increase with increasing the iodine content, which is in good agreement with the PEC measurements. These results confirm the good optoelectronic property of our NWs.

Conclusions

In summary, we have developed a facile solution-based method for the synthesis of highly uniform single-crystalline $Bi_{19}S_{27}(Br_{3-x},I_x)$ alloyed NWs across the whole composition range ($0 \le x \le 3$) with the aid of foreign metal ions (Al^{3+}). A systematic increase in the lattice constant values with substitution I^- for Br^- in $Bi_{19}S_{27}Br_3$ confirms the formation of $Bi_{19}S_{27}(Br_{3-x},I_x)$ alloyed NWs. The as-synthesized NWs shows an unusual composition-independent band gap of ~0.82 eV which is mainly due to the small contributions of halogen to the valence band maximum and conduction band minimum. Photoelectrochemical measurement reveals that the $Bi_{19}S_{27}(Br_{3-x},I_x)$ NWs are p-type semiconductor and sensitive to light irradiation. Moreover, PDs made of these NWs exhibit high sensitivity to the white light, confirming the great potential of $Bi_{19}S_{27}(Br_{3-x},I_x)$ NWs in high-performance optoelectronic devices.

Acknowledgments

We acknowledge the financial support from the National Basic Research Program of China (No. 2013CB933500, 2012CB932400), the Natural Science Foundation of China (No. 21322202 and 20873141) and the "Hundred Talents Program" of the Chinese Academy of Sciences.

Notes and references

1 (a) N. P. Dasgupta, J. Sun, C. Liu, S. Brittman, S. C. Andrews, J. Lim, H. Gao, R. Yan and P. Yang, *Adv. Mater.*, 2014, **26**, 2137; (b) A. I. Hochbaum and P. Yang, *Chem. Rev.*, 2010, **110**, 527.
2 F. Qian, S. Gradečak, Y. Li, C.-Y. Wen and C. M. Lieber, *Nano Lett.*, 2005, **5**, 2287.
3 (a) T. J. Kempa, R. W. Day, S.-K. Kim, H.-G. Park and C. M. Lieber, *Energy Environ. Sci.*, 2013, **6**, 719; (b) S. Liu, X. Guo, M. Li, W.-H. Zhang, X. Liu and C. Li, *Angew. Chem., Int. Ed.*, 2011, **50**, 12050.
4 (a) J. Miao, W. Hu, N. Guo, Z. Lu, X. Zou, L. Liao, S. Shi, P. Chen, Z. Fan, J. C. Ho, T.-X. Li, X. S. Chen and W. Lu, *ACS Nano*, 2014, **8**, 3628; (b) G. Chen, B. Liang, X. Liu, Z. Liu, G. Yu, X. Xie, T. Luo, D. Chen, M. Zhu, G. Shen and Z. Fan, *ACS Nano*, 2014, **8**, 787; (c) J.-J. Wang, Y.-Q. Wang, F.-F. Cao, Y.-G. Guo and L.-J. Wan, *J. Am. Chem. Soc.*, 2010, **132**, 12218.
5 L. Li, H. Lu, Z. Yang, L. Tong, Y. Bando and D. Golberg, *Adv. Mater.*, 2013, **25**, 1109.
6 H. Fang, T. Feng, H. Yang, X. Ruan and Y. Wu, *Nano Lett.*, 2013, **13**, 2058.
7 E. W. Wong, P. E. Sheehan and C. M. Lieber, *Science*, 1997, **277**, 1971.
8 Y. Xia, P. Yang, Y. Sun, Y. Wu, B. Mayers, B. Gates, Y. Yin, F. Kim and H. Yan, *Adv. Mater.*, 2003, **15**, 353.
9 (a) G. Meng, T. Yanagida, K. Nagashima, H. Yoshida, M. Kanai, A. Klamchuen, F. Zhuge, Y. He, S. Rahong, X. Fang, S. Takeda and T. Kawai, *J. Am. Chem. Soc.*, 2013, **135**, 7033; (b) M. Heurlin, M. H. Magnusson, D. Lindgren, M. Ek, L. R. Wallenberg, K. Deppert and L. Samuelson, *Nature*, 2012, **492**, 90; (c) H.-Y. Tuan, D. C. Lee and B. A. Korgel, *Angew. Chem., Int. Ed.*, 2006, **45**, 5184.
10 (a) J. Joo, B. Y. Chow, M. Prakash, E. S. Boyden and J. M. Jacobson, *Nat. Mater.*, 2011, **10**, 596; (b) F. Meng, S. A. Morin and S. Jin, *J. Am. Chem. Soc.*, 2011, **133**, 8408.
11 (a) C. Wang, Y. Hu, C. M. Lieber and S. Sun, *J. Am. Chem. Soc.*, 2008, **130**, 8902; (b) J. Tang, ZiyangHuo, S. Brittman, H. Gao and P. Yang, *Nat. Nanotechonol.*, 2011, **6**, 568.
12 (a) C. O'Sullivan, R. D. Gunning, A. Sanyal, C. A. Barrett, H. Geaney, F. R. Laffir, S. Ahmed and K. M. Ryan, *J. Am. Chem. Soc.*, 2009, **131**, 12250; (b) N. Pradhan, H. Xu and X. Peng, *Nano Lett.*, 2006, **6**, 720; (c) K.-S. Cho, D. V. Talapin, W. Gaschler and C. B. Murray, *J. Am. Chem. Soc.*, 2005, **127**, 7140.
13 (a) X. Zhang, N. Bao, K. Ramasamy, Y.-H. A. Wang, Y. Wang, B. Lin and A. Gupta, *Chem. Commun.*, 2012, **48**, 4956; (b) Y. Zou, X. Su and J. Jiang, *J. Am. Chem. Soc.*, 2013, **135**, 18377; (c) M. E. Norako, M. J. Greaney and R. L. Brutchey, *J. Am. Chem. Soc.*, 2012, **134**, 23.
14 (a) K. P. Rice, A. E. Saunders and M. P. Stoykovich, *J. Am. Chem. Soc.*, 2013, **135**, 6669; (b) Y.-H. A. Wang, X. Zhang, N. Bao, B. Lin and A. Gupta, *J. Am. Chem. Soc.*, 2011, **133**, 11072; (c) X. Peng, L. Manna, W. Yang, J. Wickham, E. Scher, A. Kadavanich and A. P. Alivisatos, *Nature*, 2000, **404**, 59; (d) W. Zhou, M. Yao, L. Guo, Y. Li, J. Li and S. Yang, *J. Am. Chem. Soc.*, 2009, **131**, 2959; (e) J. Nai, Y. Tian, X. Guan and L. Guo, *J. Am. Chem. Soc.*, 2013, **135**, 16082.
15 (a) C. Yang, B. Zhou, S. Miao, C. Yang, B. Cai, W.-H. Zhang and X. Xu, *J. Am. Chem. Soc.*, 2013, **135**, 5958; (b) A. Singh, S. Singh, S. Levcenko, T. Unold, F. Laffir and K. M. Ryan, *Angew. Chem., Int. Ed.*, 2013, **52**, 9120; (c) Y. Wu, B. Zhou, M. Li, C. Yang, W.-H. Zhang and C. Li, *Chem. Commun.*, 2014, **50**, 12738.
16 (a) L. Wu, B. Quan, Y. Liu, R. Song and Z. Tang, *ACS Nano*, 2011, **5**, 2224; (b) W. Han, L. Yi, N. Zhao, A. Tang, M. Gao and Z. Tang, *J. Am. Chem. Soc.*, 2008, **130**, 13152.
17 (a) J.-j. Wang, P. Liu, C. C. Seaton and K. M. Ryan, *J. Am. Chem. Soc.*, 2014, **136**, 7954; (b) Z. Li and X. Peng, *J. Am. Chem. Soc.*, 2011, **133**, 6578; (c) E. A. Weiss, *Acc. Chem. Res.*, 2013, **46**, 2607.
18 (a) W. Li, R. Zamani, P. Rivera Gil, B. Pelaz, M. Ibáñez, D. Cadavid, A. Shavel, R. A. Alvarez-Puebla, W. J. Parak, J. Arbiol and A. Cabot, *J. Am. Chem. Soc.*, 2013, **135**, 7098; (b) W. Li, R. Zamani, M. Ibáñez, D. Cadavid, A. Shavel, J. R. Morante, J. Arbiol and A. Cabot, *J. Am. Chem. Soc.*, 2013, **135**, 4664.
19 (a) Y. Wu, B. Yuan, M. Li, W.-H. Zhang, Y. Liu and C. Li, *Chem. Sci.*, 2015, **6**, 1873; (b) V. Krämer, *J Appl Crystallogr*, 1973, **6**, 499; (c) L. Zhu, Y. Xie, X. Zheng, X. Yin and X. Tian, *Inorg. Chem.*, 2002, **41**, 4560; (d) C. Deng, H. Guan and X. Tian, *Mater. Lett.*, 2013, **108**, 17.
20 K. Mariolacos, *Mater. Res. Bull.*, 2004, **39**, 591.
21 (a) L. Vegard and H. Schjelderup, *Phys. Z.*, 1917, **18**, 93; (b) M. D. Regulacio and M.-Y. Han, *Acc. Chem. Res.*, 2010, **43**, 621.
22 (a) K. Ai, Y. Liu, J. Liu, Q. Yuan, Y. He and L. Lu, *Adv. Mater.*, 2011, **23**, 4886; (b) J. Grigas, E. Talik and V. Lazauskas, *phys. stat. sol. (b)*, 2002, **232**, 220.
23 H. Li, Q. Zhang, A. Pan, Y. Wang, B. Zou and H. J. Fan, *Chem. Mater.*, 2011, **23**, 1299.
24 Y. Zhao, K. T. E. Chua, C. K. Gan, J. Zhang, B. Peng, Z. Peng and Q. Xiong, *Phys. Rev. B*, 2011, **84**, 205330.
25 G. A. Bowmaker, J. M. Harrowfield, P. C. Junk, B. W. Shelton and A. H. White, *Aust J Chem*, 1998, **51**, 285.
26 (a) G. Kresse and J. Furthmüller, *Comput. Mater. Sci.*, 1996, **6**, 15; (b) G. Kresse and J. Furthmüller, *Phys. Rev. B*, 1996, **54**, 11169.
27 (a) P. E. Blöchl, *Phys. Rev. B*, 1994, **50**, 17953; (b) G. Kresse and D. Joubert, *Phys. Rev. B*, 1999, **59**, 1758.
28 J. P. Predew, K. Burke and M. Ernzerhof, *Phys. Rev. Lett.*, 1996, **77**, 3865.
29 D. H. Webber and R. L. Brutchey, *J. Am. Chem. Soc.*, 2012, **134**, 1085.

Table of contents

Highly uniform single-crystalline $Bi_{19}S_{27}(Br_{3-x},I_x)$ alloyed nanowires (NWs) ($0 \leq x \leq 3$) were achieved for the first time, the NWs show a composition-independent band gap and great application potential in optoelectronic devices.